Improving Ground-Level NO_2 Estimation in China Using GEMS Measurements and a Nested Machine Learning Model

Naveed Ahmad[1], Changqing Lin[1,*], Alexis K.H. Lau,[1,2] Jhoon Kim[3], Fangqun Yu[4], Chengcai Li[5], Ying Li[6], Jimmy C.H. Fung[1,7], Xiang Qian Lao[8]

5   [1]Division of Environment and Sustainability, The Hong Kong University of Science and Technology, Clear Water Bay, Hong Kong, China

[2]Department of Civil and Environmental Engineering, The Hong Kong University of Science and Technology, Clear Water Bay, Hong Kong, China

[3]Department of Atmospheric Sciences, Yonsei University, Seoul, 03722, Korea

10   [4]Atmospheric Sciences Research Center, State University of New York at Albany, Albany, NY 12226, US

[5]Department of Atmospheric and Oceanic Sciences, School of Physics, Peking University, Beijing 100871, China

[6]Department of Ocean Science and Engineering, Southern University of Science and Technology, Shenzhen 518055, China

[7]Department of Mathematics, The Hong Kong University of Science and Technology, Clear Water Bay, Hong Kong,
15   China

[8]Department of Biomedical Sciences, City University of Hong Kong, Hong Kong SAR, China

Correspondence to: Changqing Lin (cqlin@ust.hk)

Abstract. The major bridge linking satellite-derived vertical column densities (VCDs) of nitrogen dioxide (NO_2) with ground-level concentration is theoretically the NO_2 mixing height (NMH). Various meteorological parameters have
20   been used as a proxy of NMH in existing studies. This study developed a nested machine learning model to convert VCDs of NO_2 into ground-level NO_2 concentrations across China using Geostationary Environmental Monitoring Spectrometer (GEMS) measurements. This nested model was designed to directly incorporate NMH into the methodological framework and explore its impact on performance. The inner machine learning model predicted the NMH from the meteorological parameters, which were then input into the main machine learning model to predict the
25   ground-level NO_2 concentrations from its VCDs. The inclusion of NMH significantly enhanced the accuracy of estimating ground-level NO_2 concentration, reducing bias and improving R^2 values to 0.93 in 10-fold cross-validation and 0.99 in the fully-trained model. Furthermore, NMH was identified as the second most important predictor variable, following the VCDs of NO_2. Subsequently, satellite-derived ground-level NO_2 data were analyzed across subregions with varying geolocations and urbanization levels. Highly populated areas typically experienced peak NO_2
30   concentrations during early morning rush hours, whereas areas categorized as lightly populated observed a slight

increase in NO_2 levels one or two hours later, likely due to regional pollutant dispersion from urban sources. This study underscores the importance of incorporating NMH in estimating ground-level NO_2 from satellite column measurements and highlights the significant advantages of geostationary satellites in providing detailed air pollution information at an hourly resolution.

1 Introduction

Nitrogen dioxide (NO_2) stands as a pivotal trace gas within the atmosphere, exerting substantial influence on the ecological environment, air quality, and climate change (Myhre et al., 2013). This significance is underscored by its role as a prominent air pollutant, with inhalable characteristics that pose potential health risks (Xue et al., 2023). Additionally, it serves as an essential precursor to the formation of secondary particles and ozone (Li et al., 2019). The origins of NO_2 are multifarious and intricate. It stems from diverse sources such as fossil-fuel-fired power plants, vehicular emissions, industrial activities, biofuel combustion, and residential cooking (Jion et al., 2023). Natural sources encompass wildfires, soil emissions, and lightning discharges (Li et al., 2022). Concerted efforts, including stringent emission control policies implemented in China, have resulted in a gradual reduction of NO_2 concentrations (Fan et al., 2020). Despite these positive trends, severe NO_2 pollution issues persist due to the heavy emissions associated with China's rapid economic development, particularly in urban agglomerations (Meng et al., 2018). The polluted regions in China continue to exhibit NO_2 concentrations that surpass the safety standard set by the World Health Organization (WHO) Air Quality Guidelines (AQG) (Chi et al., 2022).

While ground-based monitoring excels in accurately capturing NO_2 concentrations, the challenge lies in the low density and scattered distribution of observation stations (Wei et al., 2022). The inherent limitations in the geographical coverage of these stations, coupled with the elevated costs, render it challenging to effectively fulfill the requirements for monitoring ground-level NO_2 concentrations across extensive regions (Kong et al., 2021). This spatial limitation introduces substantial uncertainties when endeavoring to assess the levels of exposure on a large scale (Chi et al., 2022). Satellite instruments offer continuous air quality monitoring with broad spatial coverage (Li & Managi, 2022). Satellite-retrieved vertical column densities (VCDs) of NO_2 have been extensively utilized to identify variations in NO_2 pollution and emissions of nitrogen oxides (NO_x) across various regions (Cui et al., 2021; Iqbal et al., 2022; Park et al., 2021). However, the official satellite products provide only the column amount of NO_2 (Lamsal et al., 2014). Consequently, there has been a discernible surge in scientific research focused on deriving ground-level NO_2 concentrations through satellite data analyses.

The NO_2 columns have been measured through polar sun-synchronous low earth orbiting (LEO) satellite instruments (Yang et al., 2023). These LEO satellite instruments have a daily overpassing time at exact locations. However, NO_2 pollution may vary significantly during different times of the day, driven by emission, meteorology, and atmospheric chemistry (Shen et al., 2023). The single measurement per day from the LEO satellite instruments, typically taken around noon or in the afternoon, may lead to an underestimation of annual mean values (Qin et al., 2017). Previous studies have explored the diurnal variations of NO_2 by leveraging the differences in overpass times among these LEO satellite instruments (Boersma et al., 2008; Lin et al., 2010). However, these analyses are largely affected by the varied

performance of on-board monitoring sensors and unstable data pairing (Hilboll et al., 2013). This highlights the importance of using the quantitatively uniform air quality dataset with a much higher temporal resolution from a single suite of on-board monitoring sensors to provide new insights into diurnal variation of air pollution.

The Geostationary Environment Monitoring Spectrometer (GEMS) stands as the inaugural satellite instrument launched for the explicit purpose of monitoring both gaseous and aerosol pollutants from a geostationary earth orbit (GEO) over Asia (Kim et al., 2020). It was launched successfully by the Republic of Korea on February 19, 2020, and entered its intended orbit on March 6, 2020. The primary objective of the GEMS mission is to provide hourly columnar measurements of critical air quality parameters, including NO_2, ozone, and aerosols, across the Asian region. Distinguished from traditional LEO satellite instruments, GEMS, being GEO-based, affords more frequent monitoring of the columnar concentration of air pollutants, thereby enhancing our comprehension of the diurnal variations of NO_2 over Asia (Yang et al., 2023). Additionally, the data acquired through GEMS measurements show a significant improvement in spatial resolution compared to most existing LEO measurements.

Various studies have been conducted to estimate ground-level NO_2 concentrations from satellite measurements, leveraging their ability to cover a large spatial extent (Fan et al., 2021; Qin et al., 2020; Wu et al., 2021). The major bridge linking the VCDs of NO_2 with the ground-level concentration is theoretically the NO_2 mixing height (NMH). The variations in the NMH can be governed by various meteorological conditions (Ahmad et al., 2024). For instance, increased temperature facilitates the vertical dispersion of NO_2, leading to an increase in the NMH. To convert the VCDs of NO_2 into ground-level concentrations, studies have employed various techniques, such as air quality models, machine learning techniques, land-use regression, and geographically weighted regression (Chi et al., 2022; Lamsal et al., 2008; Wei et al., 2022; Xu et al., 2021). These conversion models have considered multiple meteorological factors, such as temperature, humidity, and wind, along with the planetary boundary layer height (PBLH) (Chi et al., 2022; Qin et al., 2020; Wei et al., 2022). The PBLH has been used as a proxy of the NMH because of its ability to regulate near-surface pollution levels. However, it is important to develop a conversion model that directly consider the impacts of the NMH. This paves the way to refine the processes of converting satellite-derived columnar measurements into ground-level NO_2 concentrations (Ahmad et al., 2024).

Based on the GEMS measurements, Ahmad et al. (2024) evaluated the impacts of meteorological factors on the variations in the NMH over China and applied a machine learning method to predict the NMH from the meteorological parameters. In the present study, we developed a nested machine-learning-based model to evaluate the effects of NMH on the conversion of columnar NO_2 measurements to ground-level NO_2 concentrations. The inner machine learning model predicted the NMH from the meteorological parameters, which were then input into the main machine learning model to predict the ground-level NO_2 concentrations from its VCDs. Further, the satellite-derived ground-level NO_2 data were analyzed for subregions with different geolocations and urbanization levels. This study aims to enhance our understanding of the effects of NMH on the conversion of satellite-based columnar measurements to ground-level NO_2 concentrations. Additionally, it seeks to enrich the information of spatial and diurnal patterns of ground-level NO_2 across China using the world's first geostationary environmental satellite.

2   Study area, data, and methodology

2.1 Study area

This study investigated the spatial and temporal variations in ground-level NO_2 concentrations using GEMS monitoring and various ground measurements for 2021. The study area is illustrated in Fig. 1, covering most of China

105   between 18°N and 43°N, and 103°E and 123°E. Considering the varied characteristics of air pollution in different regions of China, we divided the study area into six subregions: North-western China (NWC, including Gansu, Ningxia, and Shaaxi); North China (NC, including Beijing, Tianjin, Hebei, Shanxi, and Inner Mongolia); Central China (CC, including Henan, Hubei, and Hunan); Eastern China (EC, including Shandong, Jiangsu, Anhui, Shanghai, Zhejiang, Jiangxi, Fujian, and Taiwan); South-western China (SWC, including Sichuan, Chongqing, Guizhou, and

110   Yunnan); and South China (SC, including Guangdong, Guangxi, and Hainan). Satellite-derived ground-level NO_2 data were analyzed across these subregions.

Figure 1: Study area and six subregions shown as different background colors. Blue circles show distributions of ground-based NO_2 monitoring stations. Yellow circles show the distributions of meteorological stations.

115   ### 2.2 GEMS VCDs of NO_2

GEMS VCDs of NO_2 from its level 2 product were employed in this study. The NO_2 VCDs retrieval algorithm is developed based on the differential optical absorption spectroscopy (DOAS) technique (Platt et al., 2008). It initially computes slant column densities (SCDs) of NO_2 within the wavelength range of 432-450 nm. Subsequently, these SCDs are transformed into VCDs using hourly air mass factors (AMFs). The nominal detection limit for the NO_2

120   VCDs is 1×10^{14} molec/cm^2, with a retrieval accuracy of 1×10^{15} molec/cm^2. NO_2 VCDs surpassing the GEMS

detection limit of 1×10^{17} molec/cm^2 were considered as noise and consequently excluded from further analysis. The nominal spatial resolution of the GEMS dataset is approximately 7 km × 7.7 km, achieved by binning two pixels of 3.5 km × 7.7 km each. Despite the irregular shape of satellite measurement pixels due to East-to-West scans, this study standardized the VCDs of NO$_2$ onto a regular grid of 0.2º × 0.4º with the same spatial extent from 08:00 AM to 03:00
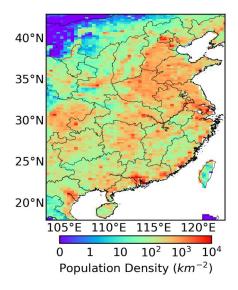125 PM local time in China. Data were excluded in the presence of cloudy conditions and solar zenith angles greater than 70^0. Additional information on the GEMS mission and retrieval algorithms is available in the study by Kim et al. (2020).

2.3 Population data

We used the latest population data for 2021 from Oak Ridge National Laboratory's (ORNL) LandScan global product
130 (https://landscan.ornl.gov). The LandScan population data is derived through an innovative methodology that combines geographic information science, remote sensing technology, and machine learning algorithms. Operating at a remarkably fine resolution of approximately 1 km, LandScan represents the most detailed global population distribution data accessible. As the satellite NO$_2$ measurements were on a regular grid of 0.2º × 0.4º, we re-gridded the LandScan population data onto a regular grid of 0.2º × 0.4º. The spatial distribution of population density (D_P, km^{-2})
135 in the study area is shown in Fig. 2. Based on population density, we divided the study region into four areas: lightly populated (LP) if $D_P \leq 200$ km^{-2}; moderately populated (MP) if $D_P > 200$ km^{-2} but ≤ 500 km^{-2}; highly populated (HP) if $D_P > 500$ km^{-2} but ≤ 1000 km^{-2}; and supremely highly populated (SHP) if $D_P > 1000$ km^{-2}. Satellite-derived ground-level NO$_2$ data were analyzed across subregions with varying urbanization levels.

Figure 2: Spatial distribution of population density (D_P, km^{-2}) within the study area.

2.4 Ground-based NO₂ and meteorological measurements

In this study, we acquired hourly NO_2 concentration data for 2021 from ground air quality monitoring networks situated within the study region. The spatial distribution of 856 ground-based NO_2 stations, sourced from the China National Environmental Monitoring Center (http://www.cnemc.cn) and the Taiwan Environmental Protection Administration (http://210.69.101.63/taqm/en/default.aspx) is shown as blue circles in Fig. 1. Meteorological variables encompassing temperature (T), air pressure (P), wind speed (WS), relative humidity (RH), dew point (DP), visibility (VIS), and precipitation (PRECIP) were used in this study. These meteorological parameters were acquired from the global telecommunications system of the World Meteorological Organization. The spatial distribution of 208 meteorological stations is illustrated as yellow circles in Fig. 1.

2.5 Locations matching between different datasets

Satellite measurements, characterized by their extensive spatial coverage, stand in contrast to the localized nature of ground measurements available at specific locations. To establish a correspondence between satellite measurements and ground air quality monitoring networks, the satellite NO_2 data specific to the geographical coordinates corresponding to ground stations were meticulously extracted. Notably, the locations of meteorological stations may differ from those of air quality monitoring stations. Therefore, meteorological data were assigned to air quality monitoring stations situated within a 50 km radius of the meteorological station. The filtering process for model training involved the selection of stations with valid observations for all meteorological and air quality variables. These station-based datasets were used to train the machine learning model. For predicting ground-level NO_2 concentrations from satellite measurements, all meteorological variables were mapped onto a regular grid of $0.2^\circ \times 0.4^\circ$ using the bilinear interpolation method. The spatial interpolation results of these meteorological parameters together with the satellite measurements on the same regular grid were employed to estimate ground-level NO_2 concentration at a resolution of $0.2^\circ \times 0.4^\circ$.

2.6 Nested machine learning model to consider the effects of NMH

Machine learning models have been successfully employed in estimating ground-level NO_2 concentrations using satellite data, typically following a two-fold procedural framework. Initializing this process involves the construction of a regression model, which is conventionally utilized to establish the overarching relationship between ground-measured NO_2 and its influencing factors (Chen et al., 2019; Chi et al., 2022). In this phase, the sample data undergoes division into a training dataset and a test dataset for model training and subsequent verification, respectively. The attainment of an optimal regression model is facilitated through parameter optimization techniques. Subsequently, the second phase entails the application of the regression model, where relevant data is inputted for application analysis to estimate the results.

Within machine learning studies, the ensemble learning paradigm emerges as a prevailing methodology to amalgamate diverse learning algorithms into a cohesive regression model characterized by robust performance across multifaceted domains. Owing to the disparate methodologies employed in the generation of individual learners, ensemble learning bifurcates into two principal categories: the sequential instantiation of individual learners, as encapsulated by the boosting approach, and the concurrent instantiation of individual learners, exemplified by bagging and Random Forest

(Friedman et al., 2000; Prasad et al., 2006). The boosting algorithm, a variant of the lifting technique, is instrumental in diminishing variance in supervised learning scenarios, wherein distinct models are formed through the employment of disparate loss functions. XGBoost leverages both first-order and second-order derivatives to enhance the precision

180   of model loss, a strategy that proves instrumental in achieving higher accuracy. Notably, during the process of selecting the optimal splitting point, XGBoost facilitates parallel optimization. This concurrent optimization significantly mitigates computational complexity, thereby effectively curtailing overfitting tendencies in the model. More details on the XGBoost regression model can be found in Chi et al. (2022). The XGBoost model was implemented in this study to convert columnar measurements into ground-level NO_2 concentrations.

185   In this study, a nested machine learning model was developed to incorporate the NMH in the conversion of columnar measurements into ground-level NO_2 concentrations. The schematic illustration of the nested machine learning model implemented in this study is depicted in Fig. 3. Firstly, an inner machine learning model (i.e., random forest) was applied to predict the NMH using meteorological variables as input parameters. The evaluation of the predicted NMH showed a good agreement with the measurement-based results, with respective coefficient of determination (R^2) values

190   of 0.84 and 0.96 for the 10-fold cross-validation and fully-trained model (Ahmad et al., 2024). The resulting NMH dataset was then mapped onto a regular grid of $0.2° \times 0.4°$ and incorporated into the main machine learning model (i.e., XGBoost regression) to estimate ground-level NO_2 concentrations. The main machine learning model employed eleven input parameters, including GEMS NO_2 VCDs, NMH, two temporal variables (i.e., month of the year ranging from 1 to 12 and hour of the day ranging from 08 AM to 03:00 PM), and seven meteorological parameters (i.e., T, P,

195   WS, RH, DP, VIS, and PRECIP). All input parameters were filtered based on available satellite observations for the year 2021. To reveal the impacts of the NMH, we compared the performance of the basic model without considering the NMH (Model I) and the nested model after considering the NMH (Model II).

To avoid overfitting and assess the efficacy of the model, the 10-fold cross-validation methodology was employed. The dataset was partitioned into 10 groups for comparable size, with nine folds utilized for model fitting and the

200   remaining fold served as a validation set to gauge model performance. This iterative process was repeated ten times, with each fold serving as the validation set, to comprehensively evaluate the model's performance across all folds. A set of widely recognized statistical metrics, including R^2, root mean squared error (RMSE), mean deviation (MD), and mean absolute percentage error (MAPE), were adopted to quantify the model's performance. In addition to the cross-validation, the XGBoost regression model was trained using the entire dataset of input parameters to predict the

205   ground-level NO_2 concentrations on a regular grid of $0.2° \times 0.4°$ across the study region for the year 2021. The fully-trained model was subsequently assessed using the same statistical indicators to comprehensively evaluate its predictive performance.
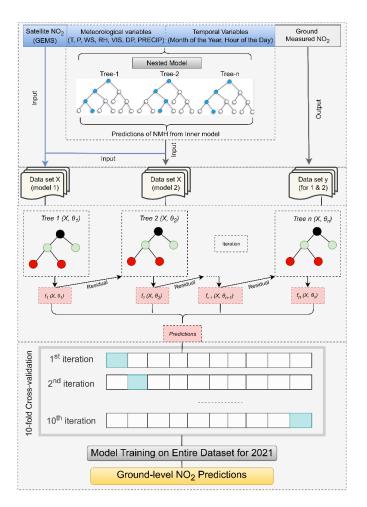
Figure 3: Schematic diagram of the nested machine learning model, including a random forest model to predict the NMH from meteorological values and an XGBoost regression model to convert the column measurements into ground-level NO$_2$ concentrations.

3 Results

3.1 Evaluations of the nested machine learning model and its feature contribution

The basic model, referred to as Model I, was trained and evaluated by considering GEMS NO$_2$ VCDs together with temporal and meteorological variables as input parameters. Then, the nested model, referred to as Model II, was trained and evaluated by considering the NMH as input parameters in addition to the input parameters of Model I. Fig. 4a shows the 10-fold cross-validation of model I. It depicts a value of 0.73 for R^2, while the RMSE, MD, and MAPE were 8.06 μg/m^3, 0.09 μg/m^3, and 39.68 %, respectively. The 10-fold cross-validation of model II after considering the NMH is revealed in Fig. 4c, which shows an improved R^2 value of 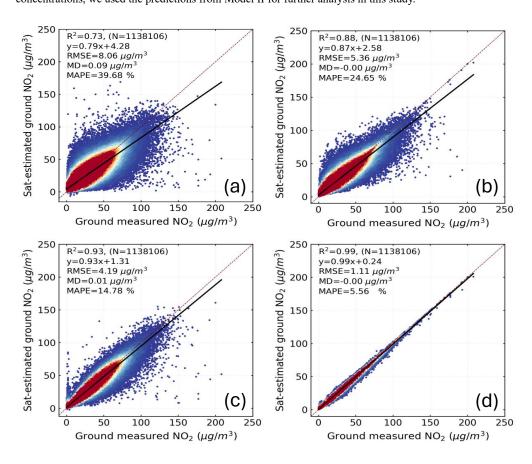0.93 and a lower RMSE of 4.19 μg/m^3, MD of 0.01 μg/m^3, and MAPE of 14.78 %. Further, we trained Model I and Model II on the entire dataset of the input

8

parameters for the year 2021. The evaluations of fully-trained Model I and Model II are presented in Fig. 4b and Fig. 4d, respectively. Again, Model II shows a lower bias and an improved R^2 value after considering the influences of NMH (e.g., R^2 increases from 0.88 to 0.99). These results clearly demonstrate that the inclusion of NMH has a great influence on the model's performance. By adding NMH as an input parameter to the machine learning model, it can

225   better capture the vertical distributions of NO_2 and hence can predict the ground-level NO_2 concentrations with higher accuracy and lower bias. Given the superior performance of Model II in accurately predicting ground-level NO_2 concentrations, we used the predictions from Model II for further analysis in this study.

Figure 4: (a) The 10-fold cross-validation of satellite-estimated ground-level NO_2 concentrations for basic Model I without
230   **considering the NMH. (b) The validation of fully-trained model for basic Model I without considering the NMH. (c) The**
10-fold cross-validation of nested Model II after considering the NMH. (d) The validation of fully-trained model for nested
Model II after considering the NMH.

A total of 11 features were involved in the predictions of ground-level NO_2. These features include GEMS NO_2 VCDs, NMH, two temporal variables (hour of the day and month of the year), and seven meteorological variables (T, P, WS,
235   RH, VIS, DP, and PRECIP). Based on the XGBoost machine learning model, the feature contribution of input parameters in descending order is presented in Fig. 5. GEMS NO_2 VCDs was identified as the top predictor variable
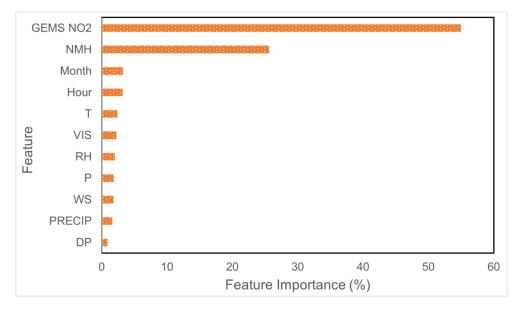
with a feature importance of 54.98 %. The second important predictor was NMH, with a contribution of 25.64 %. The temporal variables were ranked the third and fourth, with an importance of 3.23 % and 3.21 % for month of the year and hour of the day, respectively. They were followed by the meteorological parameters with a contribution of 2.45 % from temperature, 2.23 % from visibility, 2.01 % from relative humidity, 1.86 % from pressure, 1.84 % from wind speed, 1.63 % from precipitation, and 0.92 % from dew point. Among the predictors, the dominant contributors to the predictions were GEMS NO_2 VCDs and NMH, accounting for 80.62% of the predictive power. Temporal variables made a modest contribution of 6.44%, while meteorological parameters contributed 12.94% to the overall prediction accuracy.

Figure 5: Relative importance of individual input features (i.e., GEMS NO_2 VCDs, NMH, temporal variables, and meteorological parameters) in the XGBoost machine learning model.

The SHapley Additive explanations (SHAP) values presented in Fig. 6 were estimated from the XGBoost machine learning model to understand the impacts of individual input variables on the model's predictions. The analysis reveals that higher values of GEMS NO_2 VCDs correspond to higher predictions of ground-level NO_2 concentrations, while lower values of GEMS NO_2 VCDs result in lower predicted levels of ground-level NO_2. Conversely, lower NMH values are associated with higher predicted ground-level NO_2 concentrations, whereas higher NMH values are linked to lower predicted ground-level NO_2 concentrations. For temporal variables, the month of the year indicates the intra-annual pattern of ground-level NO_2, with lower concentrations observed in warm seasons and higher concentrations in cold seasons. On the other hand, the hour of the day indicates the diurnal variations of ground-level NO_2 values, with higher concentrations occurring during the morning and lower values during the afternoon. Additionally, the meteorological parameters also affect ground-level NO_2 concentrations. In general, higher atmospheric pressure is not conducive to the diffusion and dilution of NO_2, as it is generally associated with the flow moving downward in the

central area. Lower temperatures can be associated with air stagnation, leading to lower visibility and worsened
260   ground-level NO_2 pollution. Moreover, relative humidity and dew point can facilitate the conversion of NO_2 to nitrate
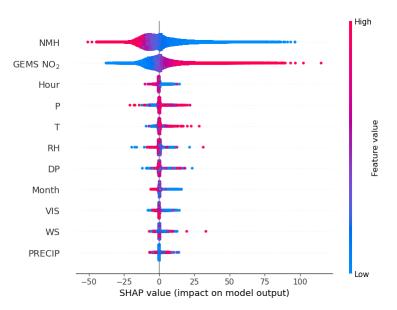and promote wet deposition processes.

Figure 6: SHapley Additive exPlanations (SHAP) values from the XGBoost machine learning model to explain the impacts of individual input variables on the model's prediction of ground-level NO_2 concentrations.

265   **3.2 Spatial distributions of ground-level NO_2 concentrations**

Based on the estimations of NO_2 concentrations for the year 2021, Fig. S1 shows an example of the spatial distributions
of ground-level NO_2 concentrations for each hour from 08:00 AM to 03:00 PM on 29 September, 2021. The figures
depict a notable diurnal pattern of ground-level NO_2, with the highest values observed at 08:00 AM and lowest values
observed at 03:00 PM, following a decreasing trend from 08:00 AM to 03:00 PM. A few GEMS NO_2 VCDs were
270   missing due to higher cloud fractions during some hours. Additionally, it should be noted that satellite measurements
are only available during the daytime. To address the data missing issues resulting from clouds and temporal gaps, we
employed a correction factor based on ground measurements. This correction factor represents the ratio between the
annual average NO_2 concentrations derived from 24-h data and the annual average NO_2 concentrations when satellite
data were available. The estimated correction factor is depicted in Fig. S2.

275   The bias-corrected NO_2 concentrations were applied in further analyses. Fig. 7 shows the spatial distributions of the
annual average ground-level NO_2 concentrations for the year 2021 across the study region, including four urban
agglomerations: Beijing-Tianjin-Hebei (BTH), Yangtze River Delta (YRD), Pearl River Delta (PRD), and Sichuan
Basin (SCB). Most urban agglomerations depicted NO_2 concentrations around 40 μg/m^3 or even higher. The highest
ground-level NO_2 concentrations were observed in the BTH region, with a spatial distribution characterized by higher
280   values in the central, southern, and southeast parts of the region, and lower concentrations in the northern and

11

southwestern areas. In the YRD region, elevated values were observed over Shanghai, the southern part of Jiangsu, and the northern part of Zhejiang. The PRD region exhibited the highest ground-level NO_2 concentrations in its central region, along with Guangdong's coast and central areas. In the SCB, the western part of Chongqing depicted the highest ground-level NO_2 concentrations, which can be attributed to its large population and higher emissions. The

285 presence of few scattered clusters of NO_2 pollution in the SCB could be attributed to economic factors and the influence of topography (Li et al., 2023). These spatial patterns are in good agreement with previous studies conducted using LEO satellite instruments (Chi et al., 2022; Qin et al., 2020; Wei et al., 2022; Wu et al., 2021; Xu et al., 2021).
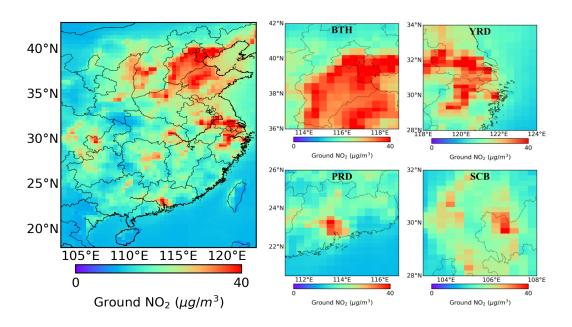

Figure 7: Spatial distributions of annual average ground-level NO_2 concentrations for 2021 in the study region (left panel)
290 **and in the four major urban agglomerations in China (right panel): Beijing-Tianjin-Hebei (BTH), Yangtze River Delta (YRD), Pearl River Delta (PRD), and Sichuan Basin (SCB).**

Considering the human health risks associated with NO_2, we evaluated the population exposure levels for different provinces in the study region. The provincial-level NO_2 concentrations were estimated from the annual average ground-level NO_2 concentrations. Fig. 8 compares the spatial mean and population-weighted mean of NO_2
295 concentrations for individual provinces in descending order by the population-weighted mean. The population-weighted mean NO_2 concentrations were consistently higher than the spatial mean NO_2 concentrations, indicating that relying solely on the spatial mean may underestimate the population exposure level. The underestimation of population exposure levels using the spatial mean was more pronounced in provinces with centralized populations (e.g., Hebei and Guangdong).

300 The population in Tianjin province was exposed to the highest levels of NO_2, with a population-weighted NO_2 mean of 40.26 μg/m³. This level of exposure is closed to the WHO Interim Target 1 (IT-1) of 40 μg/m³. The NO_2 exposure

level of people living in Hebei, Shanghai, Shandong, and Jiangsu exceeded the IT-2 levels of 30 $\mu g/m^3$. The NO_2 exposure levels for Beijing and Zhejiang were slightly under the IT-2 levels, with population-weighted means of 28.86 $\mu g/m^3$ and 28.25 $\mu g/m^3$, respectively. Residents in Henan, Anhui, Shanxi, Hubei, Sichuan, Hunan, and Jiangxi provinces were exposed to NO_2 levels exceeding the IT-3 levels of 20 $\mu g/m^3$. All provinces depicted population exposure levels of NO_2 exceeding the AQG levels of 10 $\mu g/m^3$. Hainan Province had the lowest population-weighted mean NO_2 concentrations of 10.57 $\mu g/m^3$, which closely approached the levels set by the AQG.
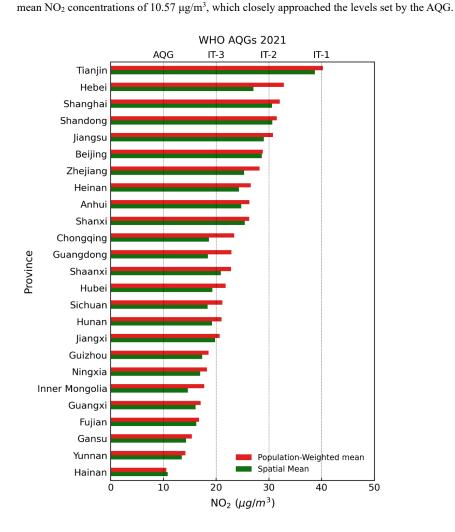

Figure 8: Spatial mean and population-weighted mean ground-level NO_2 concentrations for 2021 in different provinces of China in the study region.

The annual average ground-level NO_2 concentrations were further evaluated for all subregions with different geolocations and urbanization levels. Results are presented in Fig. 9. Overall, the highest NO_2 concentrations were observed in NC, followed by EC, CC, NWC, SWC, and SC. Additionally, compared to lightly populated areas, the

highly populated areas exhibited higher NO$_2$ concentration levels, primarily due to increased emissions and a more
315 developed economy (Qiu et al., 2023). Among all subregions, the highest NO$_2$ concentrations for highly populated
and supremely highly populated areas were found in NC region, while the highest NO$_2$ concentrations for lightly
populated areas were observed in EC region. In the highly populated areas in the NC region, NO$_2$ concentrations
exceeded IT-2 level and were nearly double the concentration of lightly populated areas. NO$_2$ concentrations in highly
populated areas of NWC, NC, CC, SWC, and SC exceeded the IT-3 levels. For moderately populated areas, only NC,
320 CC, and EC exceeded the IT-3 level. Furthermore, all the subregions and their urbanization categories, including the
lightly populated areas, depicted their NO$_2$ values higher than AQG level.
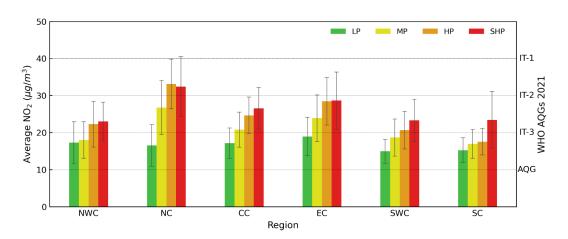

Figure 9: Annual mean ground-level NO$_2$ concentrations for 2021 in subregions with different geolocations (e.g., NWC, NC, CC, EC, SWC, and SC) and urbanization levels (e.g., LP, MP, HP, and SHP).

325 **3.3 Seasonal variations of ground-level NO$_2$ concentrations**

Similar to the annual average, the estimation of seasonal average NO$_2$ incorporated correction factors to address the
data missing issues resulting from clouds and in the nighttime (Fig. S3). Based on the bias-corrected NO$_2$ data, the
seasonal averages NO$_2$ concentrations for lightly populated, moderately populated, highly populated, and supremely
highly populated areas are shown in Fig. 10. Among all subregions, the NO$_2$ concentrations were highest in winter.
330 This can be attributed to the more stable atmospheric structure and lower precipitation during this season, which create
less favorable conditions for the dispersion and deposition of ground-level NO$_2$. Additionally, the reduced photolysis
rate of NO$_2$ due to low temperatures in winter leads to an increased residence time of NO$_2$ in the atmosphere (Xu et
al., 2021). The temperature inversion in winter can further prolong the lifetime of the ground-level NO$_2$, leading to
higher accumulations near the ground. Furthermore, the elevated concentrations in winter can be attributed to
335 increased energy consumption for heating purposes.

Among the six subregions, NC and EC depicted the highest NO$_2$ concentrations, reaching levels close to IT-1 (40
μg/m^3), in winter for highly populated areas. Conversely, the lowest ground-level NO$_2$ concentrations were observed
during summer for all six subregions. During this season, the increased precipitation coupled with the monsoon-

induced atmospheric convection foster wet deposition and dispersion of ground-level NO_2. Additionally, abundant
340   sunlight promotes the decomposition of NO_2. Furthermore, the NO_2 emissions are generally lower in summer
compared to winter (Bhattarai et al., 2021; Fan et al., 2020; Tian et al., 2019). Considering the different population
densities in the subregions, the NO_2 pollution levels were lowest in lightly populated areas and highest in highly
populated areas for all seasons. In lightly populated areas, the average NO_2 concentrations were approximately 50 %
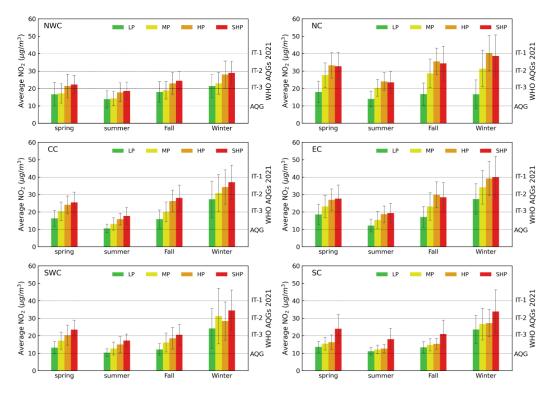of those observed in highly populated areas.

345

Figure 10: Seasonal variations in ground-level NO₂ concentrations for 2021 in subregions with different geolocations (e.g., NWC, NC, CC, EC, SWC, and SC) and urbanization levels (e.g., LP, MP, HP, and SHP).

3.4 Diurnal variations of ground-level NO₂ concentrations

The estimations of hourly average NO_2 concentrations incorporated correction factors to address data gaps caused by
350   clouds (Figs. S4 and S5). Based on the bias-corrected NO_2 data, Fig. S6 shows the spatial distribution of average
ground-level NO_2 concentrations for each hour between 08:00 AM and 03:00 PM in 2021. Consistent spatial patterns
were observed during this time range, with higher NO_2 concentrations in highly populated urban areas characterized
by elevated NO_x emissions. In the morning, clear indications of high NO_2 concentrations were noticed over urban
centers, reflecting NO_x emissions related to traffic. The spatial gradients of ground-level NO_2 concentrations were
355   notably pronounced from urban centers to outskirts during this time. However, these spatial gradients were less
pronounced during noon and afternoon hours. Compared to the highly populated urban areas, NO_2 distributions in

lightly populated areas displayed lower diurnal variability. These variations in ground-level NO_2 distributions can be attributed to changes in NO_x emission patterns, meteorological conditions, and photochemistry throughout different times of the day (Shen et al., 2023). For instance, Xu et al. (2023) observed the minimum NO_2 lifetime at noon, which

360   can be attributed to higher photochemical reaction rates resulting from increased temperature and ultraviolet radiation (Gao et al., 2023).
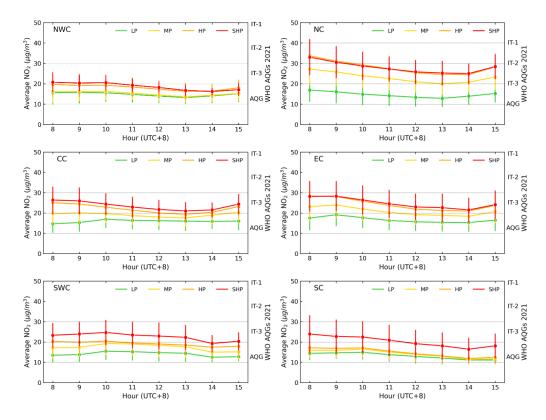
The diurnal variations of ground-level NO_2 concentrations for the subregions are illustrated in Fig. 11. In most subregions, the peak of ground-level NO_2 was observed between 08:00 AM and 09:00 AM in highly populated areas. Additionally, a slight increase in NO_2 concentrations was observed in the late afternoon (i.e., 03:00 PM). In lightly

365   populated and moderately populated areas, NWC and NC depicted a decreasing trend from 08:00 AM to 01:00 PM, followed by a slight increase at 02:00 PM and 03:00 PM. Lightly populated areas of CC showed an increasing trend from 08:00 AM to 10:00 AM, followed by a nearly constant value. However, moderately populated areas of CC showed a decreasing trend from 08:00 AM to 01:00 PM and then displayed an increasing trend at 02:00 PM and 03:00 PM. EC exhibited increasing values from 08:00 AM to 09:00 AM, followed by a decreasing trend until 02:00 PM, and

370   again increased until 03:00 PM for both lightly populated and moderately populated areas. In lightly populated and moderately populated areas of SWC, NO_2 concentrations showed an increasing trend from 08:00 AM to 10:00 AM, followed by a decreasing trend throughout the afternoon. For the SC region, NO_2 concentrations remained relatively consistent from 08:00 AM to 10:00 AM, followed by a decreasing trend in both lightly populated and moderately populated areas.

375   Overall, highly populated areas exhibited peak ground-level NO_2 concentrations during the early morning rush hours (08:00 AM - 09:00 AM), followed by a decreasing trend. The minimum NO_2 levels were observed at 01:00 PM - 02:00 PM, with a slight increase observed at 03:00 PM. This diurnal pattern of ground-level NO_2 concentrations aligns with findings by Zhang et al. (2023). The decrease in NO_2 levels from early morning to afternoon can be attributed to reduced traffic emissions, increased photochemical consumption, and higher NMH levels (Ahmad et al., 2024; Xie et

380   al., 2016). In lightly populated and moderately populated areas, a slight morning peak was observed around 09:00 AM or 10:00 AM, occurring later than the peak observed in urban areas. This delayed morning peak in these areas can be attributed to regional dispersions originating from urban sources. The diurnal pattern of ground-level NO_2 concentrations observed in this study is consistent with previous studies using ground-based air quality monitoring stations (Shen et al., 2023; Yu et al., 2020; Zhao et al., 2016).

Figure 11: Diurnal variations in ground-level NO₂ concentrations from 08:00 AM to 03:00 PM for 2021 in subregions with different geolocations (e.g., NWC, NC, CC, EC, SWC, and SC) and urbanization levels (e.g., LP, MP, HP, and SHP).

4 Discussions

GEMS, the world's first GEO-based environmental satellite instrument, offers a new opportunity for monitoring air quality across extensive regions, providing unprecedented spatial and temporal resolution. The quality of GEMS VCDs of NO₂, obtained from the level 2 product, has been evaluated using ground-based instruments in various regions. Encouragingly, a good agreement has been observed between the GEMS NO₂ VCDs and measurements from various ground-based instruments (Ahmad et al., 2024; Kim et al., 2023; Li et al., 2023). The results presented in this study emphasize the significant advantage of geostationary satellites in providing air pollution information at an hourly resolution. They enable the assessment of diurnal variations in air pollution across different areas, ranging from rural to urban regions. This represents a substantial improvement over traditional LEO-based satellite instruments. Furthermore, these GEO-based measurements serve as valuable supplements to traditional measurements from ground-based air quality monitoring networks, which are primarily concentrated in urban areas, leaving vast rural regions without observations.

NMH plays a significant role in establishing a connection between satellite column measurements and ground-level NO₂ concentrations. For example, in summer, the maximum NMH resulting from strong solar heating leads to a

dilution of ground-level pollution. Conversely, the minimum NMH in winter, caused by lower temperatures and stable atmospheric conditions, contributes to an increased accumulation of NO_2 near the surface. Additionally, diurnal variations in NMH can influence the diffusion or accumulation of ground-level NO_2. During morning hours, when NMH levels are lower, a majority of NO_2 molecules tend to accumulate near the Earth's surface. However, in the afternoon, NMH levels rise, reducing the vertical gradient of NO_2. In this study, a nested machine learning model was developed to incorporate NMH in the conversion of satellite columnar measurements to ground-level NO_2 concentrations. Two models were tested and trained: Model I, which did not consider NMH, and Model II, which incorporated NMH. The validation results demonstrated that Model II exhibited more promising outcomes than Model I, suggesting that the inclusion of NMH significantly influenced the model's performance. By including NMH as an input parameter in the machine learning model, it was better able to capture the vertical distributions of NO_2 and thus predict ground-level NO_2 concentrations with improved accuracy and performance. Furthermore, NMH was identified as the second most important predictor variable after GEMS NO_2 VCDs. Therefore, the incorporation of NMH in the machine learning model enhanced the conversion process from satellite columnar measurements to ground-level NO_2 concentrations, providing a refined and more accurate estimation.

The diurnal variations of satellite-derived ground-level NO_2 concentrations exhibit a distinct gradient across all subregions across China. In highly populated areas, peak ground-level NO_2 concentrations occur during the early morning rush hours (08:00 AM - 09:00 AM), followed by a decreasing trend with the minimum NO_2 levels observed at 01:00 PM - 02:00 PM. In lightly populated and moderately populated areas, a slight morning peak is observed around 09:00 AM or 10:00 AM, occurring later than the peak observed in urban sites. This delayed morning peak in these areas can be attributed to regional transports originating from urban sources. These diurnal variations in NO_2 levels are influenced by various driving factors, each contributing differently across different regions. For instance, anthropogenic emissions play a dominant role in highly populated urban and suburban areas, characterized by traffic emissions peaking in the morning and late afternoon (Liu et al., 2018; Naiudomthum et al., 2022). Additionally, photochemistry plays a significant role, as NO_2 is in chemical equilibrium with nitric oxide (NO). The ratio of NO_2 to NO is influenced by factors such as radiation, ozone, and peroxyl radicals. During daytime, NO_x undergoes oxidation through radical-mediated reactions, forming nitric acid and organic nitrates, with their levels depending on radiation, ozone, and volatile organic compounds. As a result, the lifetime of NO_2 reaches its lowest point around noon, typically lasting a few hours during summer. Furthermore, atmospheric transport contributes to the diurnal variation of NO_2, particularly in highly populated areas like urban centers and their surrounding regions (Zhang et al., 2023). The hourly NO_2 concentration results provide high-resolution information on the diurnal variations in NO_2 pollution levels across different regions and demographic patterns.

The annual average ground-level NO_2 concentrations revealed higher levels, reaching around 40 $\mu g/m^3$, in urban agglomerations. The provincial ranking, based on population-weighted mean NO_2 concentrations, identified the provinces along the northern and eastern coast of China (such as Tianjin and Shanghai) as having the highest NO_2 concentrations, while the provinces along the southern coast (like Hainan) exhibited the lowest concentrations. Across all subregions, ground-level NO_2 concentrations were highest in winter and lowest in summer. Additionally, the

highest NO$_2$ concentrations were observed in NC, followed by EC, CC, NWC, SWC, and SC. Despite a gradual reduction in NO$_2$ concentrations in China, most regions in China still exceeded the safety standard set by the 2021 WHO AQGs. Therefore, it is recommended to implement stringent emission controls to further reduce NO$_2$ levels and achieve a safe and acceptable air quality standard.

The ground-level NO$_2$ concentrations exhibit a clear spatial gradient, with the highest concentrations observed in highly populated areas, while minimum concentrations are found in lightly populated areas. These spatial disparities in ground-level NO$_2$ concentrations can be attributed to several factors. Firstly, the distribution of NO$_x$ emission sources varies with population densities, ranging from urban centers to rural areas. Additionally, the relatively short lifetime of NO$_2$, influenced by photolysis and chemical interactions with hydroxyl radicals, volatile organic compounds, and ozone, plays a significant role (Pusede & Cohen, 2012). The combination of mobile NO$_x$ emissions and the uneven distribution of road networks, featuring different vehicle types and traffic volumes, contributes to pronounced spatial variations in NO$_2$ levels. Moreover, the short lifespan of NO$_2$ due to atmospheric chemical reactions results in elevated concentrations in close proximity to emission sources, such as roadways, accompanied by rapid declines in NO$_2$ concentrations with increasing distance from these sources (Lee et al., 2018). Furthermore, the diverse terrains, land cover, and climates observed in different regions of China collectively influence vertical and horizontal airflows, rates of NO$_2$ formation and deposition, and contribute to spatial variations in NO$_2$.

The GEMS measurements, while valuable, are subject to uncertainties and limitations. One of the primary challenges is the impact of cloudy conditions, which can affect the reliability of GEMS measurements. To address this issue, data with a cloud fraction exceeding 30% were intentionally excluded from the analysis. This approach aimed to strike a balance between obtaining an adequate number of measurements and minimizing the influence of cloud-contaminated data. Additionally, data with a solar zenith angle exceeding 70° were excluded. Regions with a higher likelihood of cloud cover had more missing data, and there was a relatively small sample size available in the early morning due to the absence of solar radiation. Another inherent limitation of satellite measurements is the lack of data during nighttime. To ensure data quality, any VCDs exceeding 1×10^{17} molec/cm^2 were considered noise and excluded from the analysis. To align the satellite-estimated ground-level NO$_2$ concentrations with ground-measured NO$_2$ measurements, correction factors were applied for hourly, seasonal, and annual averages. Detailed information regarding these correction factors is provided in Supplement Text S1. It is important to note that the data used in this study corresponds to version 1 of the GEMS product. Ongoing efforts are being made to enhance the accuracy of GEMS products, and subsequent versions are expected to offer improved quality and reliability.

To explore the impact of missing GEMS NO$_2$ VCDs on estimating average ground-level NO$_2$ concentrations between 08:00 AM and 03:00 PM, we calculated the difference between the average NO$_2$ concentrations derived from all ground measurements and the average ground-measured NO$_2$ concentrations when satellite data was available. The hourly variations of this concentration difference for 2021 are presented in Fig. 12. The average ground-measured NO$_2$ concentrations, when satellite data was available, consistently underestimated the average NO$_2$ concentrations from all ground measurements for each hour. The degree of underestimation was higher during hours with more missing data. For instance, at 03:00 PM, 02:00 PM, 01:00 PM, and 08:00 AM, the mean underestimation was -

6.27±2.38 μg/m³, -4.38±1.94 μg/m³, -2.60±2.50 μg/m³, and -1.57±1.19 μg/m³, respectively. The underestimation
475 gradually decreased for 12:00 PM, 11:00 AM, and 09:00 AM. Notably, the underestimation was at its minimum for
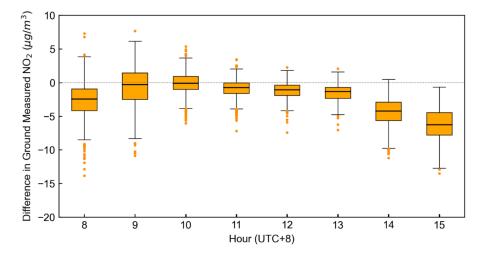10:00 AM, with a value of -0.16±1.61 μg/m³.

Figure 12: Difference between the average NO₂ concentrations from all ground measurements and the average ground-measured NO₂ concentration when satellite data was available for each hour from 08:00 AM to 03:00 PM.

480 **5 Conclusion**

In this study, a nested machine learning model was developed to incorporate the NMH as an input parameter in the
methodological framework. The model's performance in predicting ground-level NO₂ concentrations from satellite
columnar measurements was then explored. Among the testing and training of the two models, the model that
considered the NMH as one of the input parameters demonstrated more promising results. This suggests that the
485 inclusion of the NMH has a significant impact on the model's performance. Furthermore, the NMH was identified as
the second most important predictor variable after the GEMS NO₂ VCDs. The diurnal variations of satellite-derived
ground-level NO₂ concentrations exhibited a clear gradient across all subregions, ranging from highly populated areas
to lightly populated areas. In highly populated areas, peak ground-level NO₂ concentrations were observed during the
early morning rush hours (08:00 AM - 09:00 AM). In areas categorized as lightly populated or moderately populated,
490 a slight morning peak was observed around 09:00 AM or 10:00 AM, occurring later than the peak observed in urban
sites. In highly and supremely highly populated areas in northern China, NO₂ concentrations still exceeded the WHO
IT-2 standards and were double the levels observed in lightly populated regions. These satellite-derived ground-level
NO₂ concentrations provided high-resolution information on the diurnal variations of NO₂ pollution levels across
different regions and levels of urbanization. It is important to note that the GEMS measurements, while valuable, are
495 subject to uncertainties and limitations, particularly due to the impact of cloudy conditions and the absence of
nighttime data. To mitigate these issues, correction factors were applied in this study to address the inherent challenges
of satellite measurements. Overall, the findings of this study enhance our understanding of the effects of the mixing

height of NO_2 on the conversion of satellite-based columnar measurements to ground-level NO_2 concentrations. They also provide valuable insights into the spatial and diurnal patterns of ground-level NO_2 across China.

Acknowledgements

Data availability

We thank the National Institute of Environmental Research (NIER) of South Korea for providing the GEMS data (https://nesc.nier.go.kr). We thank the Institute for the Environment (IENV) and Environmental Central Facility (ENVF) of the Hong Kong University of Science and Technology (HKUST) for providing atmospheric and environmental data (http://envf.ust.hk/dataview/). Data are available upon requests.

Author Contribution

Lin CQ designed the analyses and Ahmad N carried them out. Lau AKH supervised the study. Kim J provided the data. Yu FQ and Li CC performed the simulations. Li Y, Fung JCH, and Lao XQ edited the manuscript. Ahmad N and Lin CQ prepared the manuscript with contributions from all co-authors.

Competing interests

At least one of the (co-)authors is a member of the editorial board of Atmospheric Chemistry and Physics.

Supplements

It includes Text S1 and Figs. S1-S6

References

Ahmad, N., Lin, C., Lau, A. K. H., Kim, J., Li, C., Qin, K., Zhao, C., Lin, J., Fung, J. C. H., & Li, Y.: Effects of meteorological conditions on the mixing height of Nitrogen dioxide in China using new-generation geostationary satellite measurements and machine learning. *Chemosphere*, *346, 140615.* https://doi.org/10.1016/j.chemosphere.2023.140615, 2024.

Bhattarai, H., Tripathee, L., Kang, S., Sharma, C. M., Chen, P., Guo, J., & Ghimire, P. S.: Concentration, sources and wet deposition of dissolved nitrogen and organic carbon in the Northern Indo-Gangetic Plain during monsoon. *Journal of Environmental Sciences (China)*, *102*, 37–52. https://doi.org/10.1016/j.jes.2020.09.011, 2021.

Boersma, K. F., Jacob, D. J., Eskes, H. J., Pinder, R. W., Wang, J., & van der A, R. J.: Intercomparison of SCIAMACHY and OMI tropospheric NO2 columns: Observing the diurnal evolution of chemistry and emissions from space. *Journal of Geophysical Research Atmospheres*, *113*(16). https://doi.org/10.1029/2007JD008816, 2008.

Chen, Z. Y., Zhang, R., Zhang, T. H., Ou, C. Q., & Guo, Y.: 2019 A kriging-calibrated machine learning method for estimating daily ground-level NO2 in mainland China. *Science of the Total Environment*, *690*, 556–564. https://doi.org/10.1016/j.scitotenv.2019.06.349, 2019.

Chi, Y., Fan, M., Zhao, C., Yang, Y., Fan, H., Yang, X., Yang, J., & Tao, J.: Machine learning-based estimation of ground-level NO2 concentrations over China. *Science of the Total Environment*, *807*. https://doi.org/10.1016/j.scitotenv.2021.150721, 2022.

Cui, Y., Wang, L., Jiang, L., Liu, M., Wang, J., Shi, K., & Duan, X.: Dynamic spatial analysis of NO2 pollution over China: Satellite observations and spatial convergence models. *Atmospheric Pollution Research*, *12*(3), 89–99. https://doi.org/10.1016/j.apr.2021.02.003, 2021.

Fan, C., Li, Z., Li, Y., Dong, J., Van Der A, R., & De Leeuw, G.: Variability of NO2 concentrations over China and effect on air quality derived from satellite and ground-based observations. *Atmospheric Chemistry and Physics*, *21*(10), 7723–7748. https://doi.org/10.5194/acp-21-7723-2021, 2021

Fan, H., Zhao, C., & Yang, Y.: A comprehensive analysis of the spatio-temporal variation of urban air pollution in China during 2014–2018. *Atmospheric Environment*, *220*. https://doi.org/10.1016/j.atmosenv.2019.117066, 2020.

Friedman, J., Hastie, T., & Tibshirani, R.: ADDITIVE LOGISTIC REGRESSION: A STATISTICAL VIEW OF BOOSTING. In *The Annals of Statistics* (Vol. 28, Issue 2), 2000.

Gao, Y., Pan, H., Cao, L., Lu, C., Yang, Q., Lu, X., Ding, H., Li, S., & Zhao, T.: Effects of anthropogenic emissions and meteorological conditions on diurnal variation of formaldehyde (HCHO) in the Yangtze River Delta, China. *Atmospheric Pollution Research*, *14*(6). https://doi.org/10.1016/j.apr.2023.101779, 2023.

Hilboll, A., Richter, A., & Burrows, J. P.: Long-term changes of tropospheric NO2 over megacities derived from multiple satellite instruments. *Atmospheric Chemistry and Physics*, *13*(8), 4145–4169. https://doi.org/10.5194/acp-13-4145-2013, 2013.

Iqbal, A., Ahmad, N., Din, H. M. U., Roozendael, M. Van, Anjum, M. S., Khan, M. Z. A., & Khokhar, M. F.: Retrieval of NO2 Columns by Exploiting MAX-DOAS Observations and Comparison with OMI and TROPOMI Data during the Time Period of 2015– 2019. *Aerosol and Air Quality Research*, *22*(6). https://doi.org/10.4209/aaqr.210398, 2022.

Jion, Most. M. M. F., Jannat, J. N., Mia, Md. Y., Ali, Md. A., Islam, Md. S., Ibrahim, S. M., Pal, S. C., Islam, A., Sarker, A., Malafaia, G., Bilal, M., & Islam, A. R. M. T.: A critical review and prospect of NO2 and SO2 pollution over Asia: Hotspots, trends, and sources. *Science of The Total Environment*, *876*, 162851. https://doi.org/10.1016/j.scitotenv.2023.162851, 2023.

Kim, J., Jeong, U., Ahn, M. H., Kim, J. H., Park, R. J., Lee, H., Song, C. H., Choi, Y. S., Lee, K. H., Yoo, J. M., Jeong, M. J., Park, S. K., Lee, K. M., Song, C. K., Kim, S. W., Kim, Y. J., Kim, S. W., Kim, M., Go, S., … Choi, Y.:

22

New era of air quality monitoring from space: Geostationary environment monitoring spectrometer (GEMS). *Bulletin of the American Meteorological Society*, *101*(1), E1–E22. https://doi.org/10.1175/BAMS-D-18-0013.1, 2020.

Kim, S., Kim, D., Hong, H., Chang, L. S., Lee, H., Kim, D. R., Kim, D., Yu, J. A., Lee, D., Jeong, U., Song, C. K., Kim, S. W., Park, S. S., Kim, J., Hanisco, T. F., Park, J., Choi, W., & Lee, K.: First-time comparison between NO2 vertical columns from Geostationary Environmental Monitoring Spectrometer (GEMS) and Pandora measurements. *Atmospheric Measurement Techniques*, *16*(16), 3959–3972. https://doi.org/10.5194/amt-16-3959-2023, 2023.

Kong, L., Tang, X., Zhu, J., Wang, Z., Li, J., Wu, H., Wu, Q., Chen, H., Zhu, L., Wang, W., Liu, B., Wang, Q., Chen, D., Pan, Y., Song, T., Li, F., Zheng, H., Jia, G., Lu, M., … Carmichael, G. R.: A 6-year-long (2013-2018) high-resolution air quality reanalysis dataset in China based on the assimilation of surface observations from CNEMC. *Earth System Science Data*, *13*(2), 529–570. https://doi.org/10.5194/essd-13-529-2021, 2021.

Lamsal, L. N., Krotkov, N. A., Celarier, E. A., Swartz, W. H., Pickering, K. E., Bucsela, E. J., Gleason, J. F., Martin, R. V., Philip, S., Irie, H., Cede, A., Herman, J., Weinheimer, A., Szykman, J. J., & Knepp, T. N.: Evaluation of OMI operational standard NO2 column retrievals using in situ and surface-based NO2 observations. *Atmospheric Chemistry and Physics*, *14*(21), 11587–11609. https://doi.org/10.5194/acp-14-11587-2014, 2014.

Lamsal, L. N., Martin, R. V., van Donkelaar, A., Steinbacher, M., Celarier, E. A., Bucsela, E., Dunlea, E. J., & Pinto, J. P.: Ground-level nitrogen dioxide concentrations inferred from the satellite-borne Ozone Monitoring Instrument. *Journal of Geophysical Research Atmospheres*, *113*(16). https://doi.org/10.1029/2007JD009235, 2008.

Lee, H. J., Chatfield, R. B., & Bell, M. L.: Spatial analysis of concentrations of multiple air pollutants using NASA DISCOVER-AQ aircraft measurements: Implications for exposure assessment. *Environmental Research*, *160*, 487–498. https://doi.org/10.1016/j.envres.2017.10.017, 2018.

Li, C., & Managi, S.: Estimating monthly global ground-level NO2 concentrations using geographically weighted panel regression. *Remote Sensing of Environment*, *280*. https://doi.org/10.1016/j.rse.2022.113152, 2022.

Li, K., Jacob, D. J., Liao, H., Shen, L., Zhang, Q., & Bates, K. H.: Anthropogenic drivers of 2013–2017 trends in summer surface ozone in China. *Proceedings of the National Academy of Sciences of the United States of America*, *116*(2), 422–427. https://doi.org/10.1073/pnas.1812168116, 2019.

Li, M., Mao, J., Chen, S., Bian, J., Bai, Z., Wang, X., Chen, W., & Yu, P.: Significant contribution of lightning NOx to summertime surface O3 on the Tibetan Plateau. *Science of the Total Environment*, *829*. https://doi.org/10.1016/j.scitotenv.2022.154639, 2022.

Li, Y., Xing, C., Peng, H., Song, Y., Zhang, C., Xue, J., Niu, X., & Liu, C.: Long-term observations of NO2 using GEMS in China: Validations and regional transport. *Science of the Total Environment*, *904*. https://doi.org/10.1016/j.scitotenv.2023.166762, 2023.

595   Lin, J.-T., Mcelroy, M. B., & Boersma, K. F.: Atmospheric Chemistry and Physics Constraint of anthropogenic NO x emissions in China from different sectors: a new methodology using multiple satellite retrievals. In *Atmos. Chem. Phys* (Vol. 10). www.atmos-chem-phys.net/10/63/2010/, 2010.

Liu, Y. H., Ma, J. L., Li, L., Lin, X. F., Xu, W. J., & Ding, H.: A high temporal-spatial vehicle emission inventory based on detailed hourly traffic data in a medium-sized city of China. *Environmental Pollution*, *236*, 324–333.
600   https://doi.org/10.1016/j.envpol.2018.01.068, 2018.

Meng, K., Xu, X., Cheng, X., Xu, X., Qu, X., Zhu, W., Ma, C., Yang, Y., & Zhao, Y.: Spatio-temporal variations in SO2 and NO2 emissions caused by heating over the Beijing-Tianjin-Hebei Region constrained by an adaptive nudging method with OMI data. *Science of the Total Environment*, *642*, 543–552. https://doi.org/10.1016/j.scitotenv.2018.06.021, 2018.

605   Myhre, G., D. Shindell, F.-M. Bréon, W. Collins, J. Fuglestvedt, J. Huang, D. Koch, J.-F. Lamarque, D. Lee, B. Mendoza, T. Nakajima, A. Robock, G. Stephens, T. Takemura and H. Zhang: Anthropogenic and Natural Radiative Forcing. In: Climate Change 2013: The Physical Science Basis. Contribution of Working Group I to the Fifth Assessment Report of the Intergovernmental Panel on Climate Change. Editied by Stocker, T. F. et al. Cambridge University Press, Cambridge, United Kingdom and New York, NY, USA, 2013.

610   Naiudomthum, S., Winijkul, E., & Sirisubtawee, S.: Near Real-Time Spatial and Temporal Distribution of Traffic Emissions in Bangkok Using Google Maps Application Program Interface. *Atmosphere*, *13*(11). https://doi.org/10.3390/atmos13111803, 2022.

Park, H., Jeong, S., Park, H., Labzovskii, L. D., & Bowman, K. W.: An assessment of emission characteristics of Northern Hemisphere cities using spaceborne observations of CO2, CO, and NO2. *Remote Sensing of*
615   *Environment*, *254*. https://doi.org/10.1016/j.rse.2020.112246, 2021.

Platt, U., Stutz, J., Platt, U., & Stutz, J.: Differential absorption spectroscopy (pp. 135-174). Springer Berlin Heidelberg. 10.1007/978-3-540-75776-4 6, 2008.

Prasad, A. M., Iverson, L. R., & Liaw, A.: Newer classification and regression tree techniques: Bagging and random forests for ecological prediction. *Ecosystems*, *9*(2), 181–199. https://doi.org/10.1007/s10021-005-0054-1, 2006.

620   Pusede, S. E., & Cohen, R. C.: On the observed response of ozone to NOx and VOC reactivity reductions in San Joaquin Valley California 1995-present. *Atmospheric Chemistry and Physics*, *12*(18), 8323–8339. https://doi.org/10.5194/acp-12-8323-2012, 2012.

Qin, K., Han, X., Li, D., Xu, J., Li, D., Loyola, D., Zhou, X., Xue, Y., Zhang, K., & Yuan, L.: Satellite-based estimation of surface NO2 concentrations over east-central China: A comparison of POMINO and OMNO2d data. *Atmospheric Environment*, *224*. https://doi.org/10.1016/j.atmosenv.2020.117322, 2020.

Qin, K., Rao, L., Xu, J., Bai, Y., Zou, J., Hao, N., Li, S., & Yu, C.: Estimating ground level NO2 concentrations over central-eastern China using a satellite-based geographically and temporally weighted regression model. *Remote Sensing*, *9*(9). https://doi.org/10.3390/rs9090950, 2017.

Qiu, P., Zhang, L., Wang, X., Liu, Y., Wang, S., Gong, S., & Zhang, Y.: A new approach of air pollution regionalization based on geographically weighted variations for multi-pollutants in China. *Science of the Total Environment*, *873*. https://doi.org/10.1016/j.scitotenv.2023.162431, 2023.

Shen, Y., Jiang, F., Feng, S., Xia, Z., Zheng, Y., Lyu, X., Zhang, L. Y., & Lou, C.: Increased diurnal difference of NO2 concentrations and its impact on recent ozone pollution in eastern China in summer. *Science of the Total Environment*, *858*. https://doi.org/10.1016/j.scitotenv.2022.159767, 2023.

Tian, Y., Jiang, Y., Liu, Q., Xu, D., Zhao, S., He, L., Liu, H., & Xu, H.: Temporal and spatial trends in air quality in Beijing. *Landscape and Urban Planning*, *185*, 35–43. https://doi.org/10.1016/j.landurbplan.2019.01.006, 2019.

Wei, J., Liu, S., Li, Z., Liu, C., Qin, K., Liu, X., Pinker, R. T., Dickerson, R. R., Lin, J., Boersma, K. F., Sun, L., Li, R., Xue, W., Cui, Y., Zhang, C., & Wang, J.: Ground-Level NO2Surveillance from Space Across China for High Resolution Using Interpretable Spatiotemporally Weighted Artificial Intelligence. *Environmental Science and Technology*, *56*(14), 9988–9998. https://doi.org/10.1021/acs.est.2c03834, 2022.

Wu, S., Huang, B., Wang, J., He, L., Wang, Z., Yan, Z., Lao, X., Zhang, F., Liu, R., & Du, Z.: Spatiotemporal mapping and assessment of daily ground NO2 concentrations in China using high-resolution TROPOMI retrievals. *Environmental Pollution*, *273*. https://doi.org/10.1016/j.envpol.2021.116456, 2021.

Xie, M., Zhu, K., Wang, T., Chen, P., Han, Y., Li, S., Zhuang, B., & Shu, L.: Temporal characterization and regional contribution to O 3 and NO x at an urban and a suburban site in Nanjing, China. *Science of the Total Environment*, *551–552*, 533–545. https://doi.org/10.1016/j.scitotenv.2016.02.047, 2016.

Xu, J., Lindqvist, H., Liu, Q., Wang, K., & Wang, L.: Estimating the spatial and temporal variability of the ground-level NO2 concentration in China during 2005–2019 based on satellite remote sensing. *Atmospheric Pollution Research*, *12*(2), 57–67. https://doi.org/10.1016/j.apr.2020.10.008, 2021.

Xu, T., Zhang, C., Xue, J., Hu, Q., Xing, C., & Liu, C.: Estimating Hourly Nitrogen Oxide Emissions over East Asia from Geostationary Satellite Measurements. *Environmental Science and Technology Letters*. https://doi.org/10.1021/acs.estlett.3c00467, 2023.

Xue, T., Tong, M., Wang, M., Yang, X., Wang, Y., Lin, H., Liu, H., Li, J., Huang, C., Meng, X., Zheng, Y., Tong, D., Gong, J., Zhang, S., & Zhu, T.: Health Impacts of Long-Term NO2 Exposure and Inequalities among the Chinese

655   Population from 2013 to 2020. *Environmental Science and Technology*, *57*(13), 5349–5357. https://doi.org/10.1021/acs.est.2c08022, 2023.

Yang, L. H., Jacob, D. J., Colombi, N. K., Zhai, S., Bates, K. H., Shah, V., Beaudry, E., Yantosca, R. M., Lin, H., Brewer, J. F., Chong, H., Travis, K. R., Crawford, J. H., Lamsal, L. N., Koo, J.-H., & Kim, J.: Tropospheric NO $_2$ vertical profiles over South Korea and their relation to oxidant chemistry: implications for geostationary

660   satellite retrievals and the observation of NO $_2$ diurnal variation from space. *Atmospheric Chemistry and Physics*, *23*(4), 2465–2481. https://doi.org/10.5194/acp-23-2465-2023, 2023.

Yu, S., Yin, S., Zhang, R., Wang, L., Su, F., Zhang, Y., & Yang, J.: Spatiotemporal characterization and regional contributions of O3 and NO2: An investigation of two years of monitoring data in Henan, China. *Journal of Environmental Sciences (China)*, *90*, 29–40. https://doi.org/10.1016/j.jes.2019.10.012, 2020.

665 Zhang, Y., Lin, J., Kim, J., Lee, H., Park, J., Hong, H., Van Roozendael, M., Hendrick, F., Wang, T., Wang, P., He, Q., Qin, K., Choi, Y., Kanaya, Y., Xu, J., Xie, P., Tian, X., Zhang, S., Wang, S., … Liu, M.: A research product for tropospheric NO2 columns from Geostationary Environment Monitoring Spectrometer based on Peking University OMI NO2 algorithm. *Atmospheric Measurement Techniques*, *16*(19), 4643–4665. https://doi.org/10.5194/amt-16-4643-2023, 2023.

670 Zhao, S., Yu, Y., Yin, D., He, J., Liu, N., Qu, J., & Xiao, J.: Annual and diurnal variations of gaseous and particulate pollutants in 31 provincial capital cities based on in situ air quality monitoring data from China National Environmental Monitoring Center. *Environment International*, *86*, 92–106. https://doi.org/10.1016/j.envint.2015.11.003, 2016.